



HAL
open science

Interfacial localization of CNCs in PLA/PBAT blends and its effect on rheological, thermal, and mechanical properties

Mojtaba Mohammadi, Marie-Claude Heuzey, Pierre Carreau, A. Taguet

► To cite this version:

Mojtaba Mohammadi, Marie-Claude Heuzey, Pierre Carreau, A. Taguet. Interfacial localization of CNCs in PLA/PBAT blends and its effect on rheological, thermal, and mechanical properties. *Polymer*, 2021, 233, pp.124229. 10.1016/j.polymer.2021.124229 . hal-03362458

HAL Id: hal-03362458

<https://imt-mines-ales.hal.science/hal-03362458>

Submitted on 27 Apr 2023

HAL is a multi-disciplinary open access archive for the deposit and dissemination of scientific research documents, whether they are published or not. The documents may come from teaching and research institutions in France or abroad, or from public or private research centers.

L'archive ouverte pluridisciplinaire **HAL**, est destinée au dépôt et à la diffusion de documents scientifiques de niveau recherche, publiés ou non, émanant des établissements d'enseignement et de recherche français ou étrangers, des laboratoires publics ou privés.

Interfacial localization of CNCs in PLA/PBAT blends and its effect on rheological, thermal, and mechanical properties

Mojtaba Mohammadi^a, Marie-Claude Heuzey^a, Pierre J. Carreau^{a,*}, Aurélie Taguet^b

^a Center for High Performance Polymer and Composite Systems (CREPEC), Department of Chemical Engineering, École Polytechnique de Montréal, Montreal, Québec, H3T 1J4, Canada

^b Polymers Composites and Hybrids (PCH), IMT Mines Ales, Ales, France

A B S T R A C T

In this study the effect of interfacial localization of 1 wt% cellulose nanocrystals (CNCs) was investigated on the morphology, rheology, thermal, and mechanical properties of poly (lactic acid), PLA (semicrystalline (sc) and amorphous (a)) and poly (butylene adipate-co-terephthalate), PBAT, blends (75/25 wt%). Different mixing strategies were adopted using solution casting followed by melt mixing to localize CNCs at the interface of PLA/PBAT blends. Scanning electron microscopy (SEM) and atomic force microscopy (AFM) confirmed this localization. The interfacial localization of CNCs significantly impeded the relaxation of the dispersed PBAT droplets in the PLA/PBAT blends and converted the droplet/matrix morphology of the scPLA/PBAT blend nanocomposites into a co-continuous one resulting in a solid-like rheological behavior. Also, CNCs played the role of nucleating agents in the PLA/PBAT blends and improved the crystallization behavior of scPLA and PBAT. Although Young's modulus and yield strength decreased in the neat PLA/PBAT blends, interfacial localization of CNCs improved these properties (mostly in scPLA/PBAT) to be closer to those values of neat PLAs, accompanied by improved elongation at break from ~3% (scPLA (+IMM)) to ~150% (scPLA/PBAT/CNC) and impact strength from ~20 J/m (scPLA (+IMM)) to ~95 J/m (scPLA/PBAT/CNC). These improvements were less effective in the aPLA/PBAT/CNC due to less effectiveness of CNC localization at the interface because of more residual solvent in aPLA/PBAT/CNC, better affinity of CNCs with solvent compared to polymers and more spherical PBAT dispersed phase compared to that in scPLA/PBAT/CNC blend nanocomposites.

Keywords:

PLA/PBAT/CNC nanocomposites

Interfacial localization

Rheological properties

Mechanical and thermal properties

1. Introduction

One of the most promising biodegradable polymer blend is poly (lactic acid) (PLA)/poly(butylene adipate-co-terephthalate) (PBAT) [1], where PBAT allows to give better ductility, toughness, melt strength, and processability to PLA. On the other hand, while adding PBAT to PLA may improve several properties, it may decrease the strength and modulus of the blend. Solid particles in polymer blends can help attaining a balance between toughness and stiffness [2–5]. Polymer blends containing solid particles have distinct morphologies than neat binary blends. The control of the localization of solid particles in the dispersed phase, matrix, or at the interface of the two is the most essential aspect in developing high-performance polymer blend composites. The morphology and mechanical properties are directly affected by this localization [6–8]. Nanoparticles, due to their substantially higher specific surface area, have a significant potential to improve the

mechanical and/or electrical properties at much lower particle concentrations than microparticles [7,9–11]. Several researchers have looked into the characteristics of PLA/PBAT blends with nanoparticles including nano clay [12–16], graphene [16,17], carbon nanotube [18–20], nanosilica [5,21], and cellulose nanocrystals (CNCs) [22,23]. It has been reported that the dispersed phase size in polymer blends could decrease when nanoparticles are localized in the matrix. It is explained by an increase of matrix viscosity that facilitates dispersed phase break up phenomenon [7,24,25]. Also, this localization is a well-known method for achieving a good balance of toughness and stiffness [7, 26]. When nanoparticles are localized in the dispersed phase, the viscosity and elasticity of the dispersed phase increase, hence stabilizing the morphology of the minor phase [4,27,28]. Higher nanoparticle contents in the dispersed phase could eventually lead to a co-continuous morphology [29–32]. Nanoparticle localization at the interface of polymer blends has gained a lot of interest recently [7,10,24]. It may

* Corresponding author.

E-mail address: pierre.carreau@polymtl.ca (P.J. Carreau).

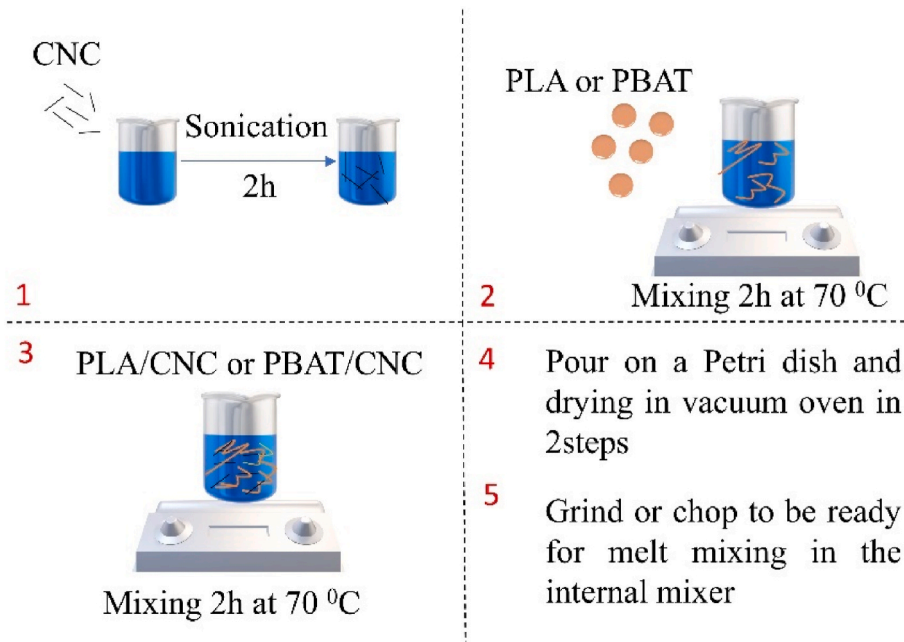


Fig. 1. PLA/CNC and PBAT/CNC neat nanocomposites preparation method. The CNC content in neat nanocomposites based on their initial localization are 1 wt%; initial localization in both phases, 1.4 wt%; initial localization in the matrix phase and 4 wt%; initial localization in the dispersed phase. Steps 1–5 are from the beginning to end of the process.

result in a reduction in the dispersed phase size via two key mechanisms: a) suppression coalescence caused by nanoparticles solid barrier effect and b) compatibilization of the blend. In the former mechanism nanoparticles create a shell around the dispersed phase, preventing colliding droplets of the dispersed phase from coalescing [33,34]. In the latter mechanism, the interaction of nanoparticles with polymer components, as well as the resulting reduction in the interfacial tension, result in blend compatibilization and a reduction in the dispersed phase size [35–37]. In a recent study, Jalali Dil et al. [5] investigated the droplet/matrix and co-continuous morphology of PLA/PBAT (70/30 and 50/50 wt% respectively) in the presence of nanosilica. They reported that adding 1 wt% nanosilica to the 70/30 wt % of PLA/PBAT blend decreases the droplet size from 1.7 to 1 μm in PLA/PBAT blends by creating a shell around PBAT droplets and acting as a barrier for coalescence. By increasing the amount of nanosilica up to 3 wt% the droplet morphology was converted to a co-continuous one. Upon these morphological changes, the rheological properties of the PLA/PBAT blends were transformed from liquid-to solid-like. On the other hand, adding 3 wt% nanosilica did not change the co-continuous morphology of PLA/PBAT (50/50). In another study conducted by Jalali Dil et al. [20], interfacial localization of 3 wt% MWCNT in the blend of PLA/PBAT (80/20 wt%) converted the dispersed phase morphology to a co-continuous one. Nofar et al. [14] investigated PLA/PBAT blends at a fixed ratio of 75/25 wt% containing Cloisite 30B. They studied the influence of shear flow on the morphology of the blend. Similarly, to thermodynamics predictions, the Cloisite 30B was localized at the interface of the two phases. The Cloisite 30B had a barrier effect on the coalescence of the droplet and stabilized the blend morphology under shear flow. It is worth mentioning that the effect of interfacial localization of nanoparticles on rheological properties of different polymer blend nanocomposites have been investigated in previous studies and they reported similar observations of dramatic increases of the complex viscosity and storage modulus at low frequencies [5,12,14,20,29,38–43]. This improvement depends on the type of nanoparticles, content, state of dispersion, as well as type of components in the blend nanocomposites [8].

Despite prior research on the effect of nanoparticle interfacial localization on the morphology and rheology of polymer blends, few

studies focused on the effect of interfacial localization of nanoparticles on the mechanical properties. This is due to the complexity of the subject, which requires a thorough examination of the morphology, rheology, and mechanical characteristics of the system. Jalali Dil et al. [5] demonstrated that 3 wt% nanosilica localized at the interface of PLA/PBAT (70/30%) blend and converted the matrix-droplet morphology to a co-continuous one. They also proved that the mechanical properties were significantly improved compared to the neat PLA, and they reported an increase from $4.2 \pm 1\%$ (PLA/3 wt% nanosilica) to $284 \pm 63\%$ (PLA/PBAT/3 wt% nanosilica) for elongation at break and from 22 ± 5 (PLA/3 wt% nanosilica) N/m to 205 ± 31 (PLA/PBAT/3 wt% nanosilica) N/m for impact strength. In another study on the effect of localization of nanoparticles on mechanical properties, Nofar et al. [23] investigated the system PLA/PBAT/CNC, prepared through solution casting (master batch approach) followed by melt mixing via a twin-screw extruder. They observed that due to the presence of remaining solvent from the solution casting preparation step the expected improved ductility and impact characteristics were not obtained. However, they did not present microscopic analysis.

In our previous study [22], the effect of CNCs on the neat nanocomposites of PLA and PBAT and their blend (PLA/PBAT (75 wt%/25 wt%) nanocomposites were investigated through morphological and rheological analyses. We observed that in some cases CNCs had a tendency to be localized at the interface of the PLA/PBAT blend [22]. In this work, the effects of interfacial localization of CNCs on the morphology, rheology, thermal, and mechanical properties of the PLA/PBAT(75 wt %/25 wt%) blend are examined. To this aim, at first, the morphology and rheology of PLA/PBAT blends with CNCs localized at the interface are examined. Secondly, thermal and mechanical properties of PLA/PBAT blends with CNCs at the interface are presented and discussed.

2. Experimental

2.1. Materials

NatureWorks LLC, USA, provided two commercially available grades, respectively amorphous and semi-crystalline linear PLAs, Ingeo 4060D (weight average molecular weight of 190 kg/mol) and 3251D

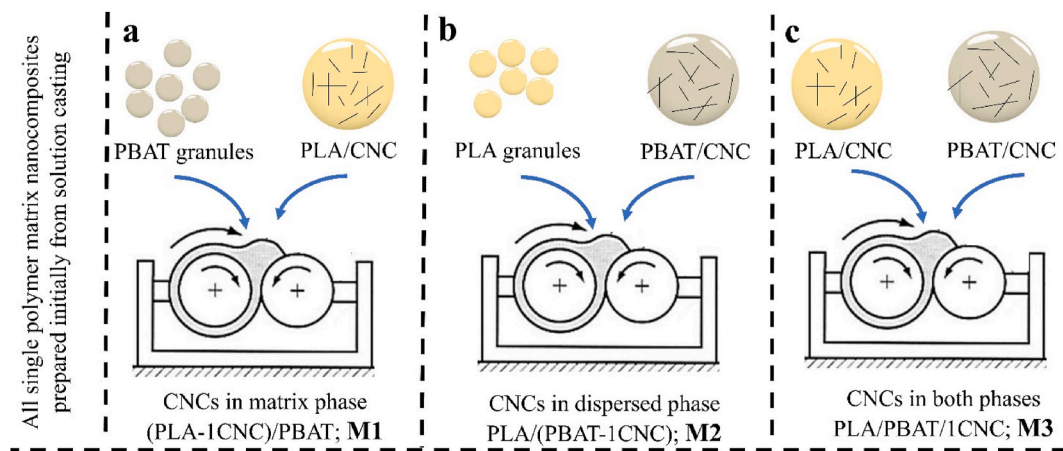


Fig. 2. Schematics of the preparation method of PLA/PBAT blend nanocomposites containing CNCs. a) M1; (PLA-1CNC)/PBAT): granules of the neat PBAT were added to PLA/1.4CNC nanocomposites, b) M2; PLA/(PBAT-1CNC): granules of the neat PLAs were added to PBAT/4CNC nanocomposites, and c) M3; PLA/PBAT/1CNC: PLA/1CNC and PBAT/1CNC nanocomposites were melted mixed.

(weight average molecular weight of 55 kg/mol), having D-lactide contents of 12% and 1.4%, respectively. Amorphous (a) and semi-crystalline (sc) PLAs are referred as aPLA and scPLA, respectively. PBAT (Ecoflex FBX 7011) was obtained from BASF and has a weight average molecular weight of 24.4 kg/mol and a melt flow index (MFI) of 2 g/10 min. Freeze-dried CNCs with width, length, and aspect ratio of 16 ± 3 , 90 ± 17 , and 6 ± 2 nm, respectively [44] were kindly provided by FPInnovations (Pointe-Claire, QC, Canada). The CNCs were neutralized using sodium hydroxide (NaOH) before freeze-drying and preparation information can be found elsewhere [45]. N, N-dimethylformamide (DMF), anhydrous 99.8%, were purchased from Sigma-Aldrich Canada Co. (Oakville, ON, Canada).

2.2. Blend nanocomposite preparation

The blend nanocomposites of PLA/PBAT (75/25 wt%) with the incorporation of 1 wt% CNCs were prepared through solution casting followed by melt mixing. Unless otherwise mentioned, PLA in the nomenclature of the neat blends or blend nanocomposites refer to both amorphous (aPLA) and semicrystalline (scPLA). The solution casting process was used to prepare the neat nanocomposites of PLA/CNC, and PBAT/CNC (Fig. 1). In the solution casting step, using a water bath sonicator and a magnetic stirrer, DMF was used to disperse and dissolve the CNCs and neat polymers, respectively. The CNCs and neat polymers were further mixed together with a magnetic stirrer after complete dispersion and dissolution. The prepared samples were dried in a vacuum oven in a two-step process [22]. For the first two days, the samples were placed in a vacuum oven (0.9 bar) with air circulation set at 60 °C. The drying process was then finished for another two days at 80 °C under vacuum (-0.65 bar). The weight percent of CNC within the nanocomposites was 1, 1.4, and 4 (PLA/1CNC, PBAT/1CNC, PLA/1.4CNC and PBAT/4CNC). More detailed information on the neat nanocomposites preparation is presented in our previous publication [22].

The melt blending of neat polymers and their nanocomposites was done in an internal mixer using a DDRV501 Brabender (C. W. Brabender Instruments Inc., South Hackensack, NJ, USA) to prepare final blend nanocomposites of PLA/PBAT containing 1 wt% of CNCs. Prior to melt mixing, all the components were dried overnight at 55 °C. Three mixing strategies were used based on the initial localization of CNCs in PLA, PBAT, or both in the solution casting step. M1) granules of the neat PBAT were added to PLA/1.4CNC nanocomposites, M2) granules of the neat PLAs were added to PBAT/4CNC nanocomposites, and M3) PLA/1CNC and PBAT/1CNC were melt mixed. The melt mixing was performed at 180 °C, 100 rpm for 7 min under a nitrogen atmosphere. The schematic

preparation method in the melt mixing step is presented in Fig. 2. In this paper based on the initial localization of CNCs, the terms (PLA-1CNC)/PBAT, PLA/(PBAT-1CNC), and PLA/PBAT/1CNC stand for samples prepared from methods M1, M2, and M3, respectively. Also, the neat PLA/PBAT blends and neat PLA from solution casting followed by internal melt mixing were prepared for comparison (PLA/PBAT (+IMM) and PLA (+IMM), respectively).

Before microscopic, rheological, thermal, and mechanical investigations, the samples were compression molded into disc (thickness of 1.2 mm and a diameter of 25 mm), rectangle, and dog-bone-shaped specimens using a hydraulic press in a nitrogen atmosphere. The compression molding process lasted 10 min at 180 °C in a nitrogen atmosphere, with 4 min of heating and 6 min of gradually rising pressure force from 1 to 3 tons. Microscopic analysis was also performed using the rheological discs.

2.3. Characterization

2.3.1. Scanning electron microscope (SEM)

The neat blends (PLA/PBAT) and their blend nanocomposites (PLA/PBAT/CNC) were fractured in liquid nitrogen to assess and compare their morphology before and after adding CNCs. The samples were subsequently covered with a 15 nm thick chromium-coated layer. At a voltage of 5 kV, the morphology was studied using an SEM (JSM 7600F, JEOL, Akishima, Tokyo 196-8558, JAPAN).

2.3.2. Atomic force microscopy (AFM)

An Ultracut FC microtome (Leica, Jung RM 2165, Concord, Ontario, Canada) with a liquid nitrogen cryo-chamber and a glass knife was used to cut and microtome samples. Using tapping mode on a Dimension ICON AFM (Bruker/Santa Barbara, CA, USA), AFM pictures were collected in the air at ambient temperature without any extra preparation. Using etched silicon cantilevers (ACTA from AppNano, Mountain View, California, USA) with a resonance frequency of roughly 300 kHz, a spring constant of 42 N/m, and a tip radius of <10 nm, intermittent contact imaging (also known as “tapping mode”) was conducted at a scan rate of 0.8 Hz. All of the photos were taken using a medium tip oscillation damping (20%–30%).

2.4. Rheological analysis

A stress/strain-controlled MCR 302 rheometer (Anton Paar, Graz, Austria) with a 25 mm parallel plate flow geometry, and a 1 mm gap was used for the rheological analysis at 180 °C under nitrogen atmosphere. Time-sweep studies at a frequency of 1 rad/s were carried out for 40 min

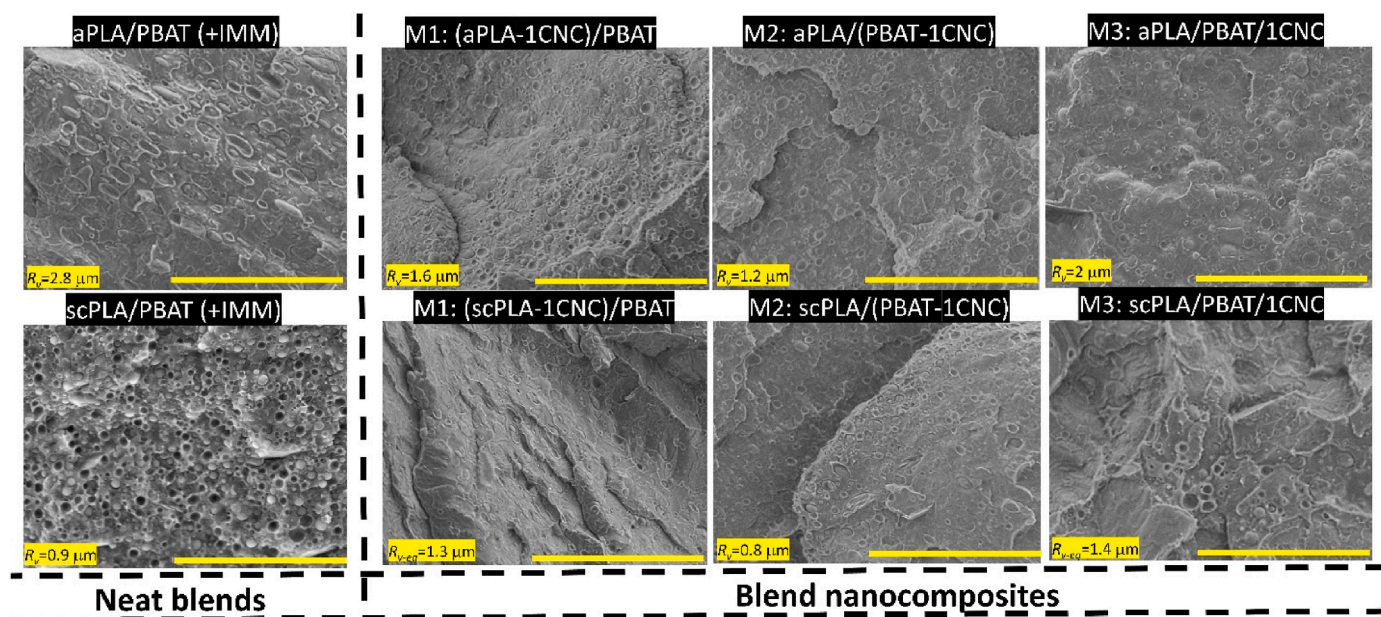


Fig. 3. SEM images of neat PLA/PBAT blends and their blend nanocomposites. M1, M2, and M3 represent the blend nanocomposites for which CNCs are initially localized in the PLA, PBAT, or both phases, respectively, in the solution casting step. The scale bars are 30 μm .

to ensure that the thermal stability of the samples was not compromised during the frequency sweep studies, which ranged from 628 rad/s to 0.05 rad/s [22]. Furthermore, strain sweep experiments were performed at a frequency of 1 rad/s on the neat polymers, polymer blend samples, and their nanocomposites to identify the linear viscoelastic area [22].

The results of time and strain sweep were presented in our previous publications [22]. The frequency sweep tests for polymer blends were carried out at a strain of 0.1%, that is in the linear viscoelastic range.

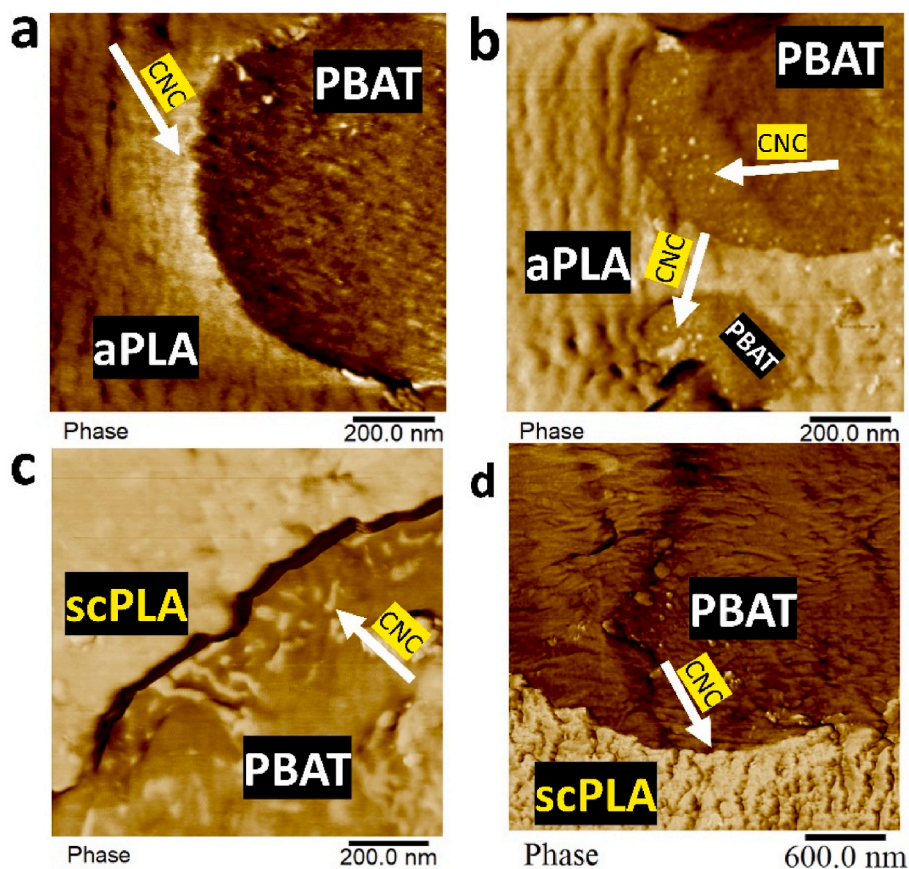


Fig. 4. Localizations of CNCs at the interface of PLA/PBAT (75/25 wt%) blend nanocomposites: AFM images of blend with 1 wt% of CNCs prepared using M1 (a and c; (PLA-1CNC)/PBAT) and M3 (b and d; PLA/PBAT/1CNC).

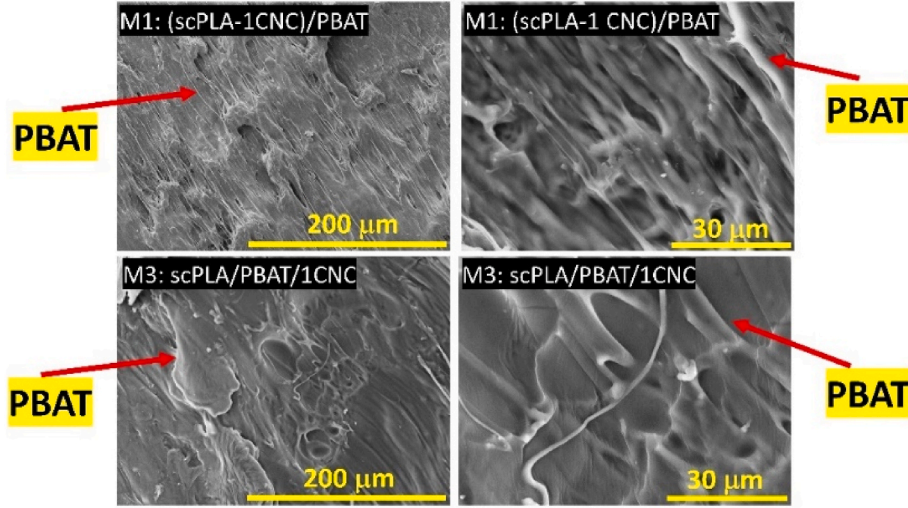


Fig. 5. SEM images for two magnifications of scPLA/PBAT/CNC prepared from M1 and M3.

2.5. Thermal analysis

Differential scanning calorimetry (DSC) was done on 5 mg material samples using a DSCQ1000 (TA Instruments, New Castle, DE, USA) in a nitrogen atmosphere. The blend nanocomposites samples were heated at a constant rate of 10 °C/min from –50 to 200 °C, kept at 200 °C for 3 min, and then cooled at a constant rate of 5 °C/min to –50 °C. In the second run, the samples were heated at a steady rate of 10 °C/min from –50 to 200 °C. For the neat PLA initial temperature was started at 25 °C. The glass transition temperature (T_g), melt and cold crystallization temperatures (T_c and T_{cc} , respectively), and crystal melting temperature (T_m) were all thoroughly investigated. The total crystallinity content was calculated using the following equations:

$$X_c^{heating} = \frac{\Delta H_m - \Delta H_{cc}}{w \times \Delta H_m} \times 100$$

$$X_c^{cooling} = \frac{\Delta H_c}{w \times \Delta H_m} \times 100$$

where w , ΔH_m , ΔH_{cc} , ΔH_m^0 , and ΔH_c are the weight fraction of the polymeric matrix in the nanocomposite, enthalpy of melting, enthalpy of cold crystallization, enthalpy of melting of 100% crystalline polymer (93 J/g [46] and 114 J/g [47] for PLA and PBAT, respectively), and enthalpy of crystallization in cooling run.

2.6. Mechanical analysis

The tensile properties of the samples at room temperature were investigated using an Instron 3365 following ASTM D638. Tensile specimens, dog bone-shaped type V with a thickness of 1.6 mm, were stretched at room temperature at a crosshead speed of 5 mm/min using a 5 kN load cell. A minimum of five specimens was tested for each sample. The tensile test was investigated without using an extensometer.

The impact strength of notched Izod was determined using a Ray-Ran Universal Pendulum Impact Tester following ASTM D256. Impact testing specimens were $63.5 \times 12.7 \times 3.0 \text{ mm}^3$ in size, and a minimum of five specimens was tested.

3. Result and discussion

3.1. Morphology

The thermodynamics equilibrium localization of CNCs in PLA/PBAT blend nanocomposites was determined to be in the PBAT phase in our

previous work [22]. This localization was determined using surface energies of the components (PLA, PBAT, and CNCs) in the blend nanocomposites and related interfacial tensions calculated from the harmonic and geometric mean equations as well as using the Palierne model [22]. Fig. 3 depicts SEM images of neat PLA/PBAT blends and their blend nanocomposites. The addition of CNCs reduces the PBAT droplet size (volume average radius, R_v) in aPLA/PBAT blend nanocomposites no matter the mixing strategy (Fig. 3, first row), but in the scPLA/PBAT blend nanocomposites (Fig. 3, second row), the PBAT droplet, R_v , decreases in the M2, while in the M1 and M3 it results in elongated PBAT droplets with a tendency for the scPLA matrix to convert the emulsion-type morphology to a co-continuous structure (more visible for M1). These morphological changes in M1 and M3 are discussed in the next paragraph and presented clearly in Fig. 5. More information about the volume average diameter determination of PBAT droplets is given in our previous work [22].

Changing the mixing strategy can result in varied localizations of CNCs. To assess the localization of the CNCs, AFM analysis (Fig. 4) at higher magnifications was done on the aPLA/PBAT/CNC (Fig. 4a and b) and scPLA/PBAT/CNC (Fig. 4c and d) blend nanocomposites prepared through M1 (Fig. 4a and c) and M3 (Fig. 4b and d). The CNCs appear as white spots or rods as indicated by arrows in these images [28,48]. The white spots correspond to the transverse sections of CNC particles. Mixing strategy M2 favors the localization of CNCs in the PBAT. When CNCs were initially dispersed in PLA (M1) or both phases (M3), they have a tendency to localize at the PLA/PBAT interface (Fig. 4), which was shown in our previous work to be an advantage for droplet coalescence barrier and blend morphological stabilization [22]. In fact, in M1 and M3, CNCs initially localized in the matrix (PLA) phase migrate partly to the interface of PLA/PBAT blends and some to the PBAT phase. The interfacial localization in aPLA/PBAT/CNC results in a size decrease of droplets of PBAT dispersed phase. The decrease in the dispersed phase size caused by nanoparticle interfacial localization has previously been reported in the literature and is attributed to a decrease in coalescence due to the solid shell of nanoparticles surrounding the dispersed phase [5,7,24]. On the other hand, Fig. 5 shows the dispersed droplet-type morphology in scPLA/PBAT/CNC prepared through M1 (Fig. 5, first row) and M3 (Fig. 5, second row) that appears to be converted to a co-continuous morphology as a result of interfacial localization of CNCs in the scPLA/PBAT/CNC (Fig. 4c and d), which could have a significant impact on the final mechanical properties of the blend nanocomposites. Selective extraction of each phase is widely used to determine the degree of phase continuity in a polymer mixture [49]. Due to the close solubility properties of the scPLA and PBAT polymers, this approach is not

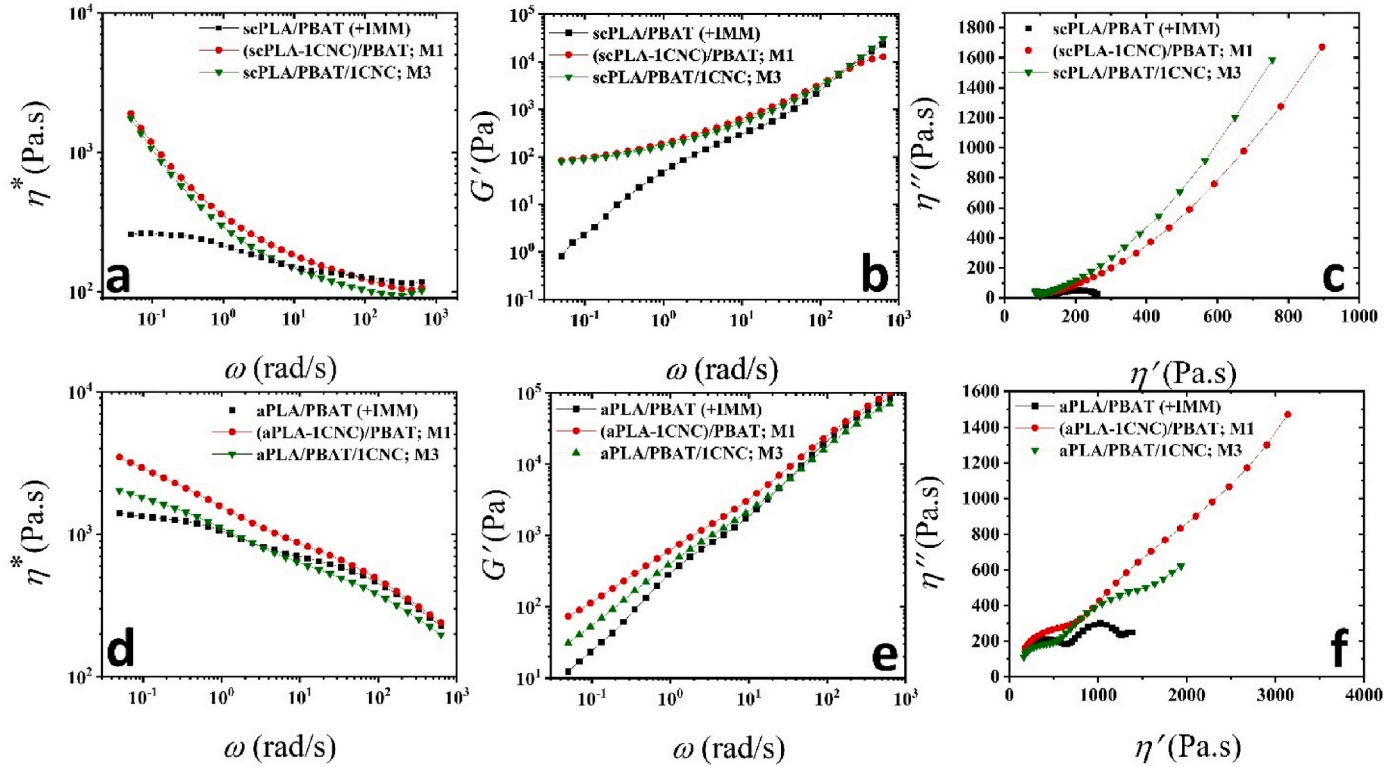


Fig. 6. Effect of interfacial localization of CNCs on (a and d) complex viscosity (b and e) storage modulus, and (c and f) Cole-Cole plots of PLA/PBAT (75/25 wt%) blend nanocomposites.

applicable in scPLA/PBAT blend. The most useful tool for the blend nanocomposites of scPLA/PBAT/CNC could be rheological analysis presented later in Fig. 6 and with related discussion.

When CNCs are introduced to the blend nanocomposites through the PBAT phase (M2), they remain in the PBAT droplets, and the results are of less interest. As a result, throughout the rest of this article, M1 ((PLA-1CNC)/PBAT) and M3 (PLA/PBAT/1CNC)) will be used as the primary mixing approach to localize CNCs at the PLA/PBAT interface and related rheological, thermal, and mechanical properties will be discussed only for these mixing strategies.

3.2. Rheological properties

Previous research [50–52] has shown that the rheological properties of PLA/PBAT blends can provide useful information on the morphology of the system. Fig. 6 depicts the influence of CNC interfacial localization (M1 and M3) on the rheological parameters (complex viscosity (a & d), storage modulus (b & e), and Cole-Cole plots (c & f)) of a PLA/PBAT (75/25 wt%) blend nanocomposites containing CNCs. When CNCs were added to aPLA or scPLA during the solution casting step (M1), the complex viscosity at low frequencies of scPLA/PBAT/CNC nanocomposites increase sharply, but the corresponding increase for aPLA/PBAT/CNC is only slight (Fig. 6a and d). At low frequencies, considerable slope reductions in the storage modulus are also found (Fig. 6b and e), primarily for scPLA/PBAT/CNC (Fig. 6b). What is more, while Fig. 6a and b shows identical rheological behavior for scPLA/PBAT/CNC prepared by M1 and M3, slightly higher values of the complex viscosity (Fig. 6d) and the storage modulus (Fig. 6e) in aPLA/PBAT/CNC observed for M1 could be due to the existence of finer morphology compared to M3 (volume average diameter of 1.6 and 2 μm for M1 and M3, respectively, reported in our previous publication [22]). These results are in accordance with the SEM analysis presented in Figs. 3 and 5. The presence of a shoulder in G' and an arc on the right side of the Cole-Cole plots of the neat blend (Fig. 6, squares) is an indication of the

dispersed phase relaxation and the existence of a matrix-droplet morphology in the sample [53]. Both the shoulder in G' (more obvious for scPLA/PBAT/CNC) and the droplet relaxation arc in the Cole-Cole plots disappear following the interfacial localization of 1 wt% CNCs (Figs. 6b–f). According to Fig. 3 for aPLA/PBAT/CNC (M1 and M3) this interfacial localization does not change the matrix-droplet morphologies. So, disappearance of the second arc of Cole-Cole plots and shoulder in storage modulus of aPLA/PBAT/CNC (M1 and M3, Fig. 6e and f) is an indication that the time of relaxation of the PBAT dispersion phase is greatly reduced. This behavior as a result of interfacial localization of nanoparticles in polymer blends has been reported in the literature [5,54,55]. On the other hand, Fig. 5 shows that for scPLA/PBAT/CNC blend nanocomposites, the interfacial localization of 1 wt% CNCs change the matrix-droplet morphology to a continuous structure of PBAT in scPLA matrix. Due to the localization of CNC combined with the continuous structure of PBAT, both the shoulder in the storage modulus and relaxation arc in the Cole-Cole plot of scPLA/PBAT/CNC disappears (Fig. 6b & c). This is due to the fact that CNCs obstruct the relaxation and mobility of polymer chains near the interface [55]. In addition, the low frequency data show a plateau in the storage modulus and a considerable upturn in complex viscosity, indicating a transition to gel-like behavior (Fig. 6a and b). Similar behavior has been reported by Jalali Dil et al. [5] when 3 wt% of nano silica were localized at the interface of PLA/PBAT blend (70/30 wt%). This behavior is remarkably similar to that reported for bicontinuous interfacial jammed emulsions (Bijels) [56,57]. The creation of a 2D network of solid particles at the interface of the co-continuous emulsion is responsible for the gel-like behavior. Therefore, the flow and deformation of the system is limited by this 2D network of CNCs at the interface and cause a gel-like behavior. These observations confirm a shift from matrix-droplet morphology to a co-continuous one observed in Fig. 5 by interfacial localization of CNCs in scPLA/PBAT/CNC.

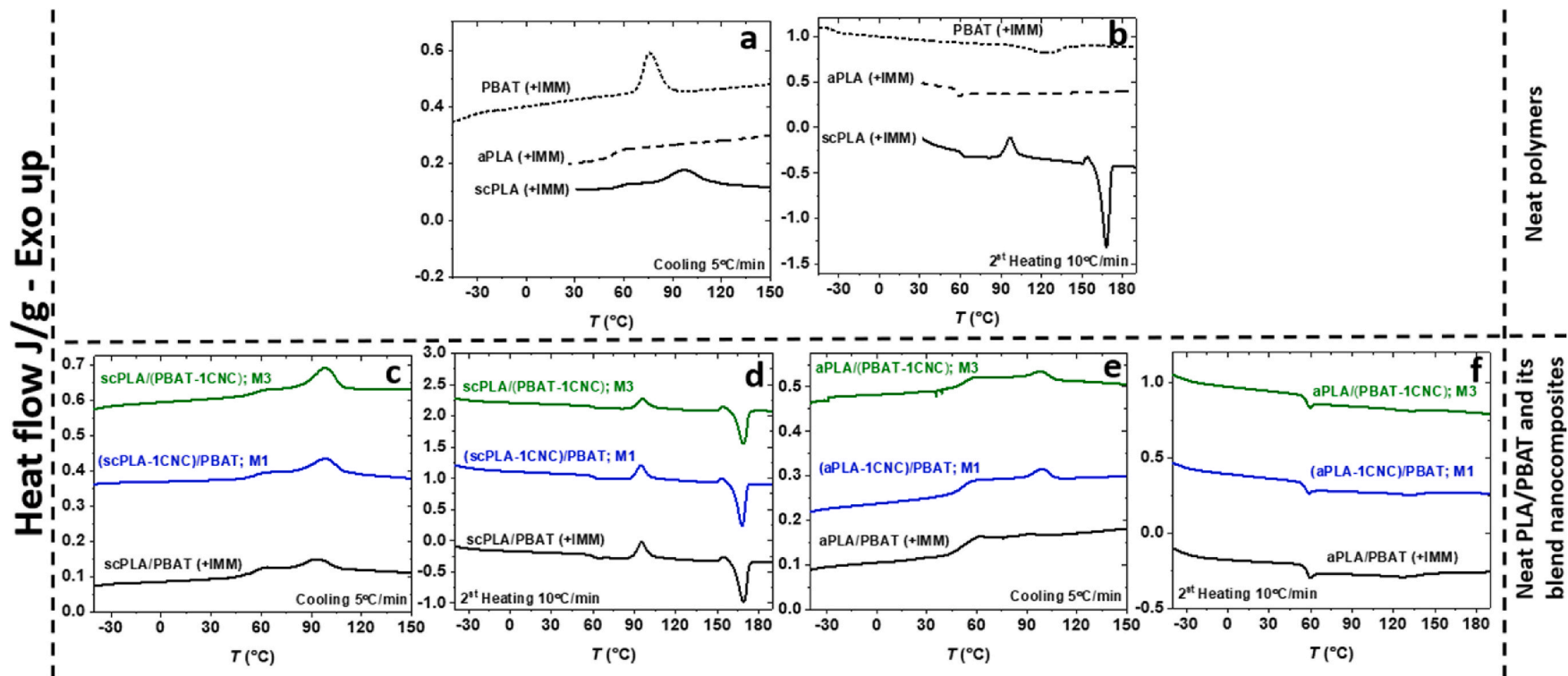


Fig. 7. DSC thermograms of first cooling (a, c, and e), and second heating (b, d, and f) sequences for a & b) scPLA (+IMM), aPLA (+IMM), and PBAT (+IMM), and c-f) neat PLA/PBAT (+IMM) blends and their blend nanocomposites prepared from M1 ((PLA-1CNC)/PBAT) and M3 (PLA/PBAT/1CNC)).

Table 1

DSC results for cooling and second heating sequences of neat PLA (+IMM), neat PLA/PBAT (+IMM), and PLA/PBAT blend nanocomposites prepared through M1 and M3.

Samples	Glass transition temperatures (°C)		Melt Crystallization temperatures (°C)	Cold crystallization temperatures (°C)	Crystal melting temperatures (°C)	Degree of crystallinity (X%)	
	$T_g^{cooling}$	$T_g^{h_2}$	T_c	T_{cc}	$T_m^{h_2}$	$X_c^{cooling}$	$X_c^{h_2}$
scPLA (+IMM)	57	59	96	95	168	14	38
scPLA/PBAT (+IMM)	57	58	94	95	169	9	18
(scPLA-1CNC)/PBAT; M1	57	59	100	96	168	18	25
aPLA/PBAT/1CNC; M3	57	59	99	96	169	18	24
aPLA (+IMM)	53	58
aPLA/PBAT (+IMM)	50	57
(aPLA-1CNC)/PBAT; M1	52	57
aPLA/PBAT/1CNC; M3	53	58

$T_g^{cooling}$: glass transition temperature of the cooling cycle; $T_g^{h_2}$: glass transition temperature of the second heating cycle; T_c : melt crystallization temperature of the cooling cycle; T_{cc} : cold crystallization temperature of the second heating cycle; $T_m^{h_2}$: crystal melting temperature of the second heating cycle; $X_c^{cooling}$: degree of crystallinity of the cooling cycle; $X_c^{h_2}$: degree of crystallinity of the second heating cycle.

3.3. Differential scanning calorimetry (DSC)

Fig. 7a and b shows the DSC thermograms of the neat polymers (aPLA (+IMM), scPLA (+IMM), and PBAT (+IMM)). The glass transition temperatures (T_g) of scPLA (+IMM), aPLA (+IMM), and PBAT (+IMM) are 57, 53, -36 °C, respectively, from the cooling cycles, and the crystal melting temperature (T_m) of scPLA (+IMM) and PBAT (+IMM) appear to be at 168 and 128 °C, respectively, from the second heating cycle (Table 1 or Fig. 7a and b). Because the presence of crystalline regions in scPLA (+IMM) hinders the molecular mobility of the amorphous part, a higher T_g is observed when compared to aPLA (+IMM). scPLA (+IMM) shows around 14 and 38% for the degree of crystallinity in the cooling cycle ($X_c^{cooling}$) and second heating cycle.

($X_c^{h_2}$) thermograms (Table 1 and Fig. 7a and b). The crystallization behavior of the neat PLA/PBAT (+IMM) blends and their blend nanocomposites (PLA/PBAT/CNC; M1 and M3) were also investigated using DSC and the results of the cooling and second heating cycles are presented in Fig. 7c-f and Table 1. Because of the varied cooling profiles applied to the samples during processing, the first heating thermograms do not provide accurate information in all of the samples and are not presented here. By the addition of CNCs, the T_g of scPLA does not change through the cooling and second heating cycles for scPLA/PBAT (+IMM) blends (Table 1). Interestingly, the T_g of aPLA in the neat aPLA/PBAT (+IMM) and its blend nanocomposites increase by about 6 °C from the cooling cycle to the second heating cycle (Table 1) [58]. This could be because the effect of remaining solvent in the melting process is more influential in aPLA/PBAT/CNC compared to scPLA/PBAT/CNC. Therefore, the aPLA/PBAT chains has more free volume in the presence of more residual solvent and exhibits a lower T_g for aPLA in the cooling cycle. Also, Similar to scPLA, the calculated T_g of PBAT (+IMM) (Fig. 7a and b; -36 °C) does not change in neat PLA/PBAT blends and their blend nanocomposites (Fig. 7c-f).

Table 1 shows that the melt crystallization temperature (T_c) of scPLA/PBAT (+IMM) decreases to 94 °C compared to 96 °C for scPLA (+IMM). Although this decrease is not significant and could be within experimental errors, more importantly, the crystallinity of scPLA (+IMM) in the cooling cycle ($X_c^{cooling}$) decreases from 14% to 9% for scPLA/PBAT (+IMM) (similar decreasing effect in the second heating cycle ($X_c^{h_2}$)) (Table 1). Hence, these reductions can be attributed to the effect of PBAT droplets as chain mobility restriction. Similar observation have been reported by Al-Itry et al. [59] for PLA/PBAT blends.

To discuss on the effect of CNC on the crystallization of scPLA, it must be noticed here that scPLA and PBAT crystallized at 75 and 96 °C (Fig. 7a). Also, it was proven elsewhere that [59] PBAT decreases the

crystallinity and the melt crystalline temperature of PLA [59] and CNC has a tendency to restrict the mobility of PBAT chains and the crystallinity of PBAT in the presence of CNC was decreased [60]. Although cold crystallization temperature (T_{cc}) does not change for scPLA/PBAT/CNC, the melt crystallization temperature (T_c) increases modestly from 94 °C in neat scPLA/PBAT (+IMM) to around 100 °C for both (scPLA-1CNC)/PBAT; M1, and scPLA/PBAT/1CNC; M3. This shows that CNCs in scPLA/PBAT/CNC act as nucleating agents that accelerate the crystallization of the scPLA in the blend nanocomposite. Moreover, the effect of CNCs as a nucleating agent is obvious in the crystallinity of scPLA in the cooling cycle ($X_c^{cooling}$). The $X_c^{cooling}$ increases from 9% in neat scPLA/PBAT (+IMM) to 18% (100% increase) in both (scPLA-1CNC)/PBAT (M1) and scPLA/PBAT/1CNC (M3) (similar increasing effect in the second heating cycle ($X_c^{h_2}$)) (Table 1). What is more, although crystallization of scPLA and PBAT are at different temperatures (96 and 75 °C, respectively; Fig. 7a) and c and d shows scPLA and PBAT crystallized at identical temperatures in the blend nanocomposites, suggesting that the PLA slow crystallization could be promoted by droplets of PBAT in addition to the presence of CNCs as nucleating agents. In other words, scPLA and PBAT crystallized simultaneously, allowing them to enhance each other crystallization and interfacial contacts between matrix and dispersed-phase molecules in a synergistic manner. Therefore, degree of crystallinity obtained for scPLA in Table 1 is affected by possible crystals of PBAT. Finally, the melting temperature of scPLA/PBAT (+IMM) blend nanocomposites are not affected by the addition of CNCs and are around 168 °C (Table 1).

Regarding the DSC of blends based on aPLA, and as mentioned in other articles, CNC do not play any nucleating role for this aPLA [61]. Moreover, PBAT hinders the mobility of PLA chains [59]. Hence, the exothermic peak that are seen in Fig. 7e is due to the crystallization of PBAT. The crystallization temperature of PBAT was increased from 81 °C for the blend to 100 °C for both (aPLA-1CNC)/PBAT; M1, and aPLA/PBAT/1CNC; M3 (Fig. 7f and g). Moreover, the calculated degree of crystallinity in PBAT increases from 4% in the neat aPLA/PBAT (+IMM) to around 12% in (aPLA-1CNC)/PBAT; M1, and aPLA/PBAT/1CNC; M3. Also, the melting temperature of around 130 °C in Fig. 7f is the PBAT melting temperature in the blends of aPLA/PBAT (+IMM) and their nanocomposites (not affected by the addition of CNCs).

3.4. Mechanical properties

Fig. 8 reports the mechanical properties of as-received granules of PLA, PLA processed from solution casting followed by melt mixing (PLA

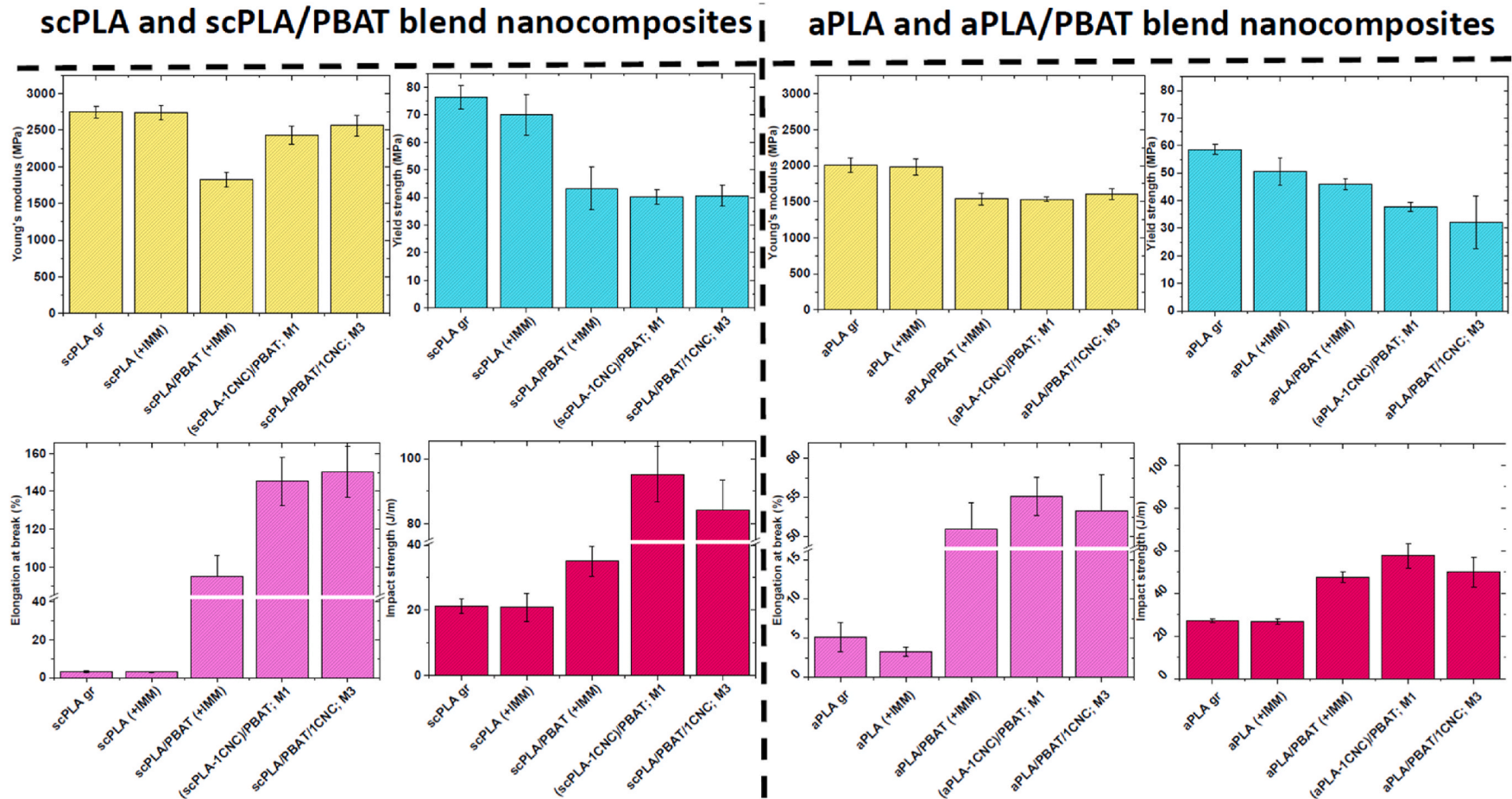


Fig. 8. Young's modulus, yield strength, elongation at break, and impact strength of granules of PLA, neat PLA (+IMM), neat PLA/PBAT (+IMM) blends, and PLA/PBAT/CNC blend nanocomposites prepared through M1 ((PLA-1CNC)/PBAT) and M3 (PLA/PBAT/1CNC). "gr" in the x-axis stands for neat polymers prepared from granules.

Table 2

Mechanical properties of granules of PLA, neat PLA (+IMM), neat PLA/PBAT (+IMM), and PLA/PBAT blend nanocomposites prepared through M1 and M3.

Sample	Young's modulus (MPa)	Yield strength (MPa)	Elongation at break (%)	Impact strength (J m ⁻¹)
scPLA granules	2748 ± 84	76 ± 4	3.1 ± 0.3	21 ± 2
scPLA (+IMM)	2740 ± 97	70 ± 7	3.0 ± 0.3	21 ± 4
scPLA/PBAT (+IMM)	1825 ± 101	43 ± 7	95 ± 9	35 ± 5
(scPLA-1CNC)/PBAT; M1	2430 ± 121	40 ± 2	145 ± 12	95 ± 8
scPLA/PBAT/1CNC; M3	2562 ± 146	40 ± 3	150 ± 13	84 ± 9
aPLA granules	2010 ± 100	58 ± 1	5.2 ± 2.0	27 ± 1
aPLA (+IMM)	1982 ± 110	50 ± 4	3.3 ± 0.6	27 ± 1
aPLA/PBAT (+IMM)	1535 ± 83	45 ± 1	50.0 ± 3.0	47 ± 2
(aPLA-1CNC)/PBAT; M1	1530 ± 31	37 ± 1	55.0 ± 2.4	58 ± 6
aPLA/PBAT/1CNC; M3	1609 ± 76	32 ± 9	53.0 ± 4.7	50 ± 7

(+IMM)), neat PLA/PBAT (+IMM) blends, and PLA/PBAT blend nanocomposites prepared from mixing strategies of M1 ((PLA-1CNC)/PBAT) and M3 (PLA/PBAT/1CNC). In both amorphous and semi-crystalline PLAs, a brittle behavior is obvious from Fig. 8 (high Young's modulus and low elongation at break) and the corresponding results are reported in Table 2. As expected, adding PBAT with high elongation at break (~700%) changes the mechanical behavior of PLA from brittle to ductile in the PLA/PBAT (+IMM) blends. It has been reported in the literature that increasing the content of PBAT has an increasing effect on elongation at break and impact strength of PLA, but decreases the yield strength and modulus [5,62]. Adding 25 wt% PBAT increases the elongation at break from 3 to 95% in scPLA/PBAT (+IMM) and from 3 to 50% in aPLA/PBAT (+IMM), respectively, compared to PLA (+IMM). The larger elongation at break for the scPLA/PBAT blend is linked also to the much lower yield strength after adding PBAT to scPLA (that goes from 70 to 43 MPa) compared to aPLA (that goes from 50 to 45 MPa). It means that in the case of scPLA the stress is transferred more easily to the PBAT than in the case of aPLA and this could be due to the better chemical affinity between scPLA and PBAT compared to that between aPLA and PBAT. As briefly discussed in the Supplementary Information of our previous publication [22], we expect scPLA with a low molecular weight and higher crystallinity compared to aPLA to have larger Hansen solubility parameters [63] and a smaller relative energy difference (RED) between scPLA and PBAT. However, the Young modulus and yield strength decrease from 2740 to 1825 MPa and from 70 to 43 MPa in scPLA/PBAT (+IMM) and from 1982 to 1535 MPa and 50 to 45 MPa in aPLA/PBAT (+IMM), respectively, compared to the neat PLAs (+IMM). What is more, the impact strength rises from 20 to 35 J/m in scPLA/PBAT (+IMM) and from 26 to 47 J/m in aPLA/PBAT (+IMM) compared to the neat PLAs (+IMM). As mentioned in the introduction, localization of nanoparticles at the interface can improve the adhesion between phases and, hence, enhance the elongation at break and impact strength of the blend nanocomposites, making a balance between toughness and stiffness. In the morphology and rheology sections, it is shown that mixing strategies 1 and 3 (M1; (PLA-1CNC)/PBAT and M3; (PLA/PBAT/1CNC)) lead to localization of CNCs at the interface of PLA and PBAT phases and this localization is more effective in the semi-crystalline scPLA/PBAT/CNC, which exhibits a solid-like behavior in rheology (Fig. 6a & b). The interfacial localization of 1 wt% CNCs in the

scPLA/PBAT blend nanocomposites increases the elongation at break and impact strength by 52 and 171% for M1 and 57 and 140% for M3 compared to the neat scPLA/PBAT (+IMM). A possible phenomenon for the significant improvement in elongation at break and impact properties in scPLA/PBAT (+IMM) blend can be attributed to the tendency of the matrix-droplet morphology in scPLA/PBAT (+IMM) blend to be converted into a co-continuous one in the presence of 1 wt% of CNCs in both M1 and M3 (Figs. 5 and 6a-c). This improvement is less effective in the aPLA/PBAT blend nanocomposites with elongation at break and impact strength increasing, respectively, by only 10% and 23% for M1 and 6% and 7% for M3 compared to the neat aPLA/PBAT (+IMM). In our previous publications [22,58], it was shown that the effect of traces of solvent after solution casting and drying and even after melt mixing was preventing achieving high performance in the neat polymers and blends. This effect of traces of solvent is more severe in aPLA compared to scPLA and PBAT with lower molecular weight and crystalline structure, which helped in expelling the solvent out of the samples during the drying process [22,58]. Also, in our previous publication [22], we have shown via the Hansen solubility parameter theory (HSP) that CNCs have a better affinity with DMF (relative energy difference (RED) equal or less than 1) compared to PLA and PBAT (RED more than 1). Therefore, in aPLA/PBAT/CNC that contains more residual solvent, the interactions between CNCs and solvent could be more pronounced compared to the CNC role in promoting interfacial adhesion between aPLA and PBAT. What is more, the addition of PBAT causes a reduction in the Young modulus of both scPLA/PBAT (+IMM) and aPLA/PBAT (+IMM) blends. On the other hand, while the reduction in the Young modulus by adding PBAT to the scPLA (+IMM) is largely recovered by the addition of 1 wt% CNCs, but the Young modulus in aPLA/PBAT/CNC (both M1 and M3) remains at the same level compared to the neat aPLA/PBAT (+IMM) blend. Again, it could be attributed to the presence of more residual solvent in aPLA/PBAT/CNC and also to the difference in molecular weight of scPLA and aPLA.

4. Conclusion

The influence of interfacial localization of 1 wt% CNCs on the morphology, rheology, thermal, and mechanical properties of scPLA/PBAT and aPLA/PBAT (75 wt%/25 wt%) blends was investigated. The blend nanocomposites were prepared through solution casting followed by melt mixing using an internal mixer. In the solution casting the CNCs were initially localized in the dispersed phase, matrix, or both phases to prepare neat nanocomposites, and their localization in the blends was studied after melt mixing using SEM and AFM. The initial localization of CNCs in the matrix or both phases resulted in CNCs being mostly localized at the interface after melt mixing. Rheological analysis and especially Cole-Cole plots indicated that for both M1 and M3 morphologies, the PBAT droplet relaxation was delayed. The slower relaxation of the PBAT droplets was also obvious in the storage modulus of scPLA/PBAT/CNC by the presence of a plateau at low frequencies, indicative of a transition from liquid-to solid-like behavior. It is worth mentioning that the initial localization of CNCs in the matrix and dispersed phases, which eventually led to its presence at the interface after melt mixing, converted the matrix-droplet morphology to a co-continuous one in the case of scPLA/PBAT/CNC. Due to this localization at the interface and morphological transformation, considerable improvements in elongation at break and impact properties of scPLA/PBAT were observed using only 1 wt% CNCs. These improvements were less effective in the case of aPLA/PBAT/CNC as a result of more residual solvent in that system and better affinity of CNCs with the solvent. Also, thermal analysis using DSC revealed the nucleation effect of CNCs and improvements of the crystallization temperature and the degree of crystallinity of scPLA. The interfacial localization of nanoparticles is an effective approach for stabilizing the morphological and improving mechanical characteristics of polymer blends. Moreover, this localization could pave the way for the creation of stable co-continuous structures for blends at low contents

of the minor phase.

CRedit authorship contribution statement

Mojtaba Mohammadi: Formal analysis, Investigation, Methodology, Validation, Writing – original draft, Writing – review & editing. **Marie-Claude Heuzey:** Formal analysis, Resources, Supervision, Validation, Visualization, Writing – review & editing. **Pierre J. Carreau:** Funding acquisition, Project administration, Formal analysis, Resources, Supervision, Validation, Visualization, Writing – review & editing. **Aurélie Taguet:** Formal analysis, Validation, Writing – review & editing.

Declaration of competing interest

The authors declare that they have no known competing financial interests or personal relationships that could have appeared to influence the work reported in this paper.

Acknowledgments

Financial support from the Natural Science and Engineering Research Council (NSERC) of Canada is gratefully acknowledged. The authors also wish to acknowledge the help of Dr. Helia Sojoudiasli and Mr. Matthieu Gauthier for the material preparation and processing. Finally, we wish to thank Mr. Jed Randall from NatureWorks for providing one of the PLA samples.

References

- [1] M. Nofar, D. Sacligil, P.J. Carreau, M.R. Kamal, M.-C. Heuzey, Poly (lactic acid) blends: processing, properties and applications, *Int. J. Biol. Macromol.* 125 (2019) 307–360.
- [2] Y. Yoo, L. Cui, P.J. Yoon, D.R. Paul, Morphology and mechanical properties of rubber toughened amorphous polyamide/MMT nanocomposites, *Macromolecules* 43 (2) (2010) 615–624.
- [3] H.S. Lee, P.D. Fasulo, W.R. Rodgers, D.R. Paul, TPO based nanocomposites. Part 1. Morphology and mechanical properties, *Polymer (Guildf)*. 46 (25) (2005) 11673–11689.
- [4] M. Kontopoulou, Y. Liu, J.R. Austin, J.S. Parent, The dynamics of montmorillonite clay dispersion and morphology development in immiscible ethylene-propylene rubber/polypropylene blends, *Polymer (Guildf)*. 48 (15) (2007) 4520–4528.
- [5] E. Jalali Dil, N. Virgilio, B.D. Favis, The effect of the interfacial assembly of nano-silica in poly(lactic acid)/poly(butylene adipate-Co-terephthalate) blends on morphology, rheology and mechanical properties, *Eur. Polym. J.* 85 (2016) 635–646.
- [6] A. Gödel, G. Kasaliwal, P. Pötschke, Selective localization and migration of multiwalled carbon nanotubes in blends of polycarbonate and poly(styrene-acrylonitrile), *Macromol. Rapid Commun.* 30 (6) (2009) 423–429.
- [7] A. Taguet, P. Cassagnau, J.-M. Lopez-Cuesta, Structuration, selective dispersion and compatibilizing effect of (Nano)Fillers in polymer blends, *Prog. Polym. Sci.* 39 (8) (2014) 1526–1563.
- [8] R. Salehiyan, M. Nofar, K. Malkappa, S.S. Ray, Effect of nanofillers characteristics and their selective localization on morphology development and rheological properties of melt-processed polylactide/poly(butylene adipate-co-terephthalate) blend composites, *Polym. Eng. Sci.* 60 (11) (2020) 2749–2760.
- [9] R. Salehiyan, M. Nofar, S.S. Ray, V. Ojijo, Kinetically controlled localization of carbon nanotubes in polylactide/poly(vinylidene fluoride) blend nanocomposites and their influence on electromagnetic interference shielding, electrical conductivity, and rheological properties, *J. Phys. Chem. C* 123 (31) (2019) 19195–19207.
- [10] M. Nofar, R. Salehiyan, S.S. Ray, Influence of nanoparticles and their selective localization on the structure and properties of polylactide-based blend nanocomposites, *Compos. B Eng.* 215 (2021), 108845.
- [11] E. Vatanserver, D. Arslan, M. Nofar, Polylactide cellulose-based nanocomposites, *Int. J. Biol. Macromol.* 137 (2019) 912–938.
- [12] M. Nofar, R. Salehiyan, U. Ciftci, A. Jalali, A. Durmuş, Ductility improvements of PLA-based binary and ternary blends with controlled morphology using PBAT, PBSA, and nanoclay, *Compos. B Eng.* 182 (2020), 107661.
- [13] M. Nofar, M.-C. Heuzey, P.J. Carreau, M.R. Kamal, Nanoparticle interactions and molecular relaxation in PLA/PBAT/nanoclay blends, *Exp. Res.* 1 (2020), e47.
- [14] M. Nofar, M.-C. Heuzey, P.J. Carreau, M.R. Kamal, Effects of nanoclay and its localization on the morphology stabilization of PLA/PBAT blends under shear flow, *Polymer (Guildf)* 98 (2016) 353–364.
- [15] S. Adrar, A. Habi, A. Ajji, Y. Grohens, Synergistic effects in epoxy functionalized graphene and modified organo-montmorillonite PLA/PBAT blends, *Appl. Clay Sci.* 157 (2018) 65–75.
- [16] S. Girdhep, N. Komrapit, R. Molloy, S. Lumyong, W. Punyodom, P. Worajittiphon, Effect of plate-like particles on properties of poly(lactic acid)/poly(butylene adipate-Co-terephthalate) blend: a comparative study between modified montmorillonite and graphene nanoplatelets, *Compos. Sci. Technol.* 119 (2015) 115–123.
- [17] M.S. Garg, D. Srivastava, Effect of glycidyl methacrylate (GMA) content on thermal and mechanical properties of ternary blend systems based on cardanol-based vinyl ester resin, styrene and glycidyl methacrylate, *Prog. Org. Coat.* 77 (7) (2014) 1208–1220.
- [18] S.W. Ko, M.K. Hong, B.J. Park, R.K. Gupta, H.J. Choi, S.N. Bhattacharya, Morphological and rheological characterization of multi-walled carbon nanotube/PLA/PBAT blend nanocomposites, *Polym. Bull.* 63 (1) (2009) 125–134.
- [19] J. Urquijo, N. Aranburu, S. Dagréou, G. Guerrica-Echevarria, J.I. Eguiazabal, CNT-induced morphology and its effect on properties in PLA/PBAT-Based nanocomposites, *Eur. Polym. J.* 93 (2017) 545–555.
- [20] E. Jalali Dil, M. Arjmand, I. Otero Navas, U. Sundararaj, B.D. Favis, Interface bridging of multiwalled carbon nanotubes in polylactic acid/poly(butylene adipate-Co-terephthalate): morphology, rheology, and electrical conductivity, *Macromolecules* 53 (22) (2020) 10267–10277.
- [21] E. Jalali Dil, B.D. Favis, Localization of micro- and nano-silica particles in heterophase poly(lactic acid)/poly(butylene adipate-Co-terephthalate) blends, *Polymer (Guildf)*. 76 (2015) 295–306.
- [22] M. Mohammadi, M.-C. Heuzey, P.J. Carreau, A. Taguet, Morphological and rheological properties of PLA, PBAT, and PLA/PBAT blend nanocomposites containing CNCs, *Nanomaterials* 11 (4) (2021) 857.
- [23] D.S. Sarul, D. Arslan, E. Vatanserver, Y. Kahraman, A. Durmus, R. Salehiyan, M. Nofar, Preparation and characterization of PLA/PBAT/CNC blend nanocomposites, *Colloid Polym. Sci.* 299 (6) (2021) 987–998.
- [24] F. Fenouillot, P. Cassagnau, J.-C. Majesté, Uneven distribution of nanoparticles in immiscible fluids: morphology development in polymer blends, *Polymer (Guildf)* 50 (6) (2009) 1333–1350.
- [25] J. Huitric, J. Ville, P. Médéric, M. Moan, T. Aubry, Rheological, morphological and structural properties of PE/PA/nanoclay ternary blends: effect of clay weight fraction, *J. Rheol. (N. Y. N. Y.)* 53 (5) (2009) 1101–1119.
- [26] M. Bailly, M. Kontopoulou, Preparation and characterization of thermoplastic olefin/nanosilica composites using a silane-grafted polypropylene matrix, *Polymer (Guildf)*. 50 (11) (2009) 2472–2480.
- [27] J.S. Hong, H. Namkung, K.H. Ahn, S.J. Lee, C. Kim, The role of organically modified layered silicate in the breakup and coalescence of droplets in PBT/PE blends, *Polymer (Guildf)*. 47 (11) (2006) 3967–3975.
- [28] V. Heshmati, M.R. Kamal, B.D. Favis, Cellulose nanocrystal in poly(lactic acid)/polyamide11 blends: preparation, morphology and Co-continuity, *Eur. Polym. J.* 98 (2018) 11–20.
- [29] G. Filippone, N.T. Dintcheva, F.P. La Mantia, D. Acierno, Using organoclay to promote morphology refinement and Co-continuity in high-density polyethylene/polyamide 6 blends – effect of filler content and polymer matrix composition, *Polymer (Guildf)*. 51 (17) (2010) 3956–3965.
- [30] G. Filippone, N.T. Dintcheva, D. Acierno, F.P. La Mantia, The role of organoclay in promoting Co-continuous morphology in high-density poly(ethylene)/poly(amide) 6 blends, *Polymer (Guildf)*. 49 (5) (2008) 1312–1322.
- [31] A. Nuzzo, E. Bilotti, T. Peijs, D. Acierno, G. Filippone, Nanoparticle-induced Co-continuity in immiscible polymer blends – a comparative study on bio-based PLA-PA11 blends filled with organoclay, sepiolite, and carbon nanotubes, *Polymer (Guildf)*. 55 (19) (2014) 4908–4919.
- [32] G. Wu, B. Li, J. Jiang, Carbon black self-networking induced Co-continuity of immiscible polymer blends, *Polymer (Guildf)*. 51 (9) (2010) 2077–2083.
- [33] L. Elias, F. Fenouillot, J.C. Majesté, G. Martin, P. Cassagnau, Migration of nanosilica particles in polymer blends, *J. Polym. Sci., Part B: Polym. Phys.* 46 (18) (2008) 1976–1983.
- [34] A.C. Baudouin, J. Devaux, C. Bailly, Localization of carbon nanotubes at the interface in blends of polyamide and ethylene-acrylate copolymer, *Polymer (Guildf)*. 51 (6) (2010) 1341–1354.
- [35] L. Elias, F. Fenouillot, J.C. Majesté, P. Cassagnau, Morphology and rheology of immiscible polymer blends filled with silica nanoparticles, *Polymer (Guildf)*. 48 (20) (2007) 6029–6040.
- [36] L. Elias, F. Fenouillot, J.C. Majesté, P. Alcouffe, P. Cassagnau, Immiscible polymer blends stabilized with nano-silica particles: rheology and effective interfacial tension, *Polymer (Guildf)*. 49 (20) (2008) 4378–4385.
- [37] R. Salehiyan, Y. Yoo, W.J. Choi, K. Hyun, Characterization of morphologies of compatibilized polypropylene/polystyrene blends with nanoparticles via nonlinear rheological properties from FT-rheology, *Macromolecules* 47 (12) (2014) 4066–4076.
- [38] Z. Shakouri, H. Nazockdast, H. Sadeghi Ghari, Effect of the geometry of cellulose nanocrystals on morphology and mechanical performance of dynamically vulcanized PLA/PU blend, *Cellulose* 27 (1) (2020) 215–231.
- [39] M. Shahlari, S. Lee, Mechanical and morphological properties of poly(butylene adipate-Co-terephthalate) and poly(lactic acid) blended with organically modified silicate layers, *Polym. Eng. Sci.* 52 (7) (2012) 1420–1428.
- [40] D. Wu, D. Lin, J. Zhang, W. Zhou, M. Zhang, Y. Zhang, D. Wang, B. Lin, Selective localization of nanofillers: effect on morphology and crystallization of PLA/PCL blends, *Macromol. Chem. Phys.* 212 (6) (2011) 613–626.
- [41] M.R. Aghjeh, V. Asadi, P. Mehdijabbar, H.A. Khonakdar, S.H. Jafari, Application of linear rheology in determination of nanoclay localization in PLA/EVA/clay nanocomposites: correlation with microstructure and thermal properties, *Compos. B Eng.* 86 (2016) 273–284.

- [42] X. Zhao, H. Wang, Z. Fu, Y. Li, Enhanced interfacial adhesion by reactive carbon nanotubes: New route to high-performance immiscible polymer blend nanocomposites with simultaneously enhanced toughness, tensile strength, and electrical conductivity, *ACS Appl. Mater. Interfaces* 10 (10) (2018) 8411–8416.
- [43] Z. Shakouri, H. Nazockdast, Microstructural development and mechanical performance of PLA/TPU blends containing geometrically different cellulose nanocrystals, *Cellulose* 25 (12) (2018) 7167–7188.
- [44] D. Bagheriasl, P.J. Carreau, B. Riedl, C. Dubois, W.Y. Hamad, Shear rheology of polylactide (PLA)–Cellulose nanocrystal (CNC) nanocomposites, *Cellulose* 23 (3) (2016) 1885–1897.
- [45] W.Y. Hamad, T.Q. Hu, Structure-process-yield interrelations in nanocrystalline cellulose extraction, *Can. J. Chem. Eng.* 88 (3) (2010) 392–402.
- [46] J. Ambrosio-Martín, M.J. Fabra, A. Lopez-Rubio, J.M. Lagaron, Melt polycondensation to improve the dispersion of bacterial cellulose into polylactide via melt compounding: enhanced barrier and mechanical properties, *Cellulose* 22 (2) (2015) 1201–1226.
- [47] R. Herrera, L. Franco, A. Rodríguez-Galán, J. Puiggalf, Characterization and degradation behavior of poly(butylene adipate- Co -terephthalate)S, *J. Polym. Sci. Part A Polym. Chem.* 40 (23) (2002) 4141–4157.
- [48] V. Heshmati, M.R. Kamal, B.D. Favis, Tuning the localization of finely dispersed cellulose nanocrystal in poly (lactic acid)/bio-polyamide11 blends, *J. Polym. Sci., Part B: Polym. Phys.* 56 (7) (2018) 576–587.
- [49] P. Pötschke, D.R. Paul, formation of Co-continuous structures in melt-mixed immiscible polymer blends, *J. Macromol. Sci. Polym. Rev.* 43 (1) (2003) 87–141.
- [50] M. Nofar, A. Maani, H. Sojoudi, M.C. Heuzey, P.J. Carreau, Interfacial and rheological properties of PLA/PBAT and PLA/PBSA blends and their morphological stability under shear flow, *J. Rheol. (N. Y. N. Y.)* 59 (2) (2015) 317–333.
- [51] E. Jalali Dil, P.J. Carreau, B.D. Favis, Morphology, miscibility and continuity development in poly(lactic acid)/poly(butylene adipate-Co-terephthalate) blends, *Polymer (Guildf)* 68 (2015) 202–212.
- [52] S.Y. Gu, K. Zhang, J. Ren, H. Zhan, Melt rheology of polylactide/poly(butylene adipate-Co-terephthalate) blends, *Carbohydr. Polym.* 74 (1) (2008) 79–85.
- [53] D. Graebing, R. Muller, J.F. Palierne, Linear viscoelastic behavior of some incompatible polymer blends in the melt. Interpretation of data with a model of emulsion of viscoelastic liquids, *Macromolecules* 26 (2) (1993) 320–329.
- [54] S. Vandebriel, J. Vermant, P. Moldenaers, Efficiently suppressing coalescence in polymer blends using nanoparticles: role of interfacial rheology, *Soft Matter* 6 (14) (2010) 3353–3362.
- [55] G. Filippone, G. Romeo, D. Acierno, Role of interface rheology in altering the onset of Co-continuity in nanoparticle-filled polymer blends, *Macromol. Mater. Eng.* 296 (7) (2011) 658–665.
- [56] L. Bai, J.W. Fruehwirth, X. Cheng, C.W. Macosko, Dynamics and rheology of nonpolar bijels, *Soft Matter* 11 (26) (2015) 5282–5293.
- [57] R. Altobelli, M. Salzano De Luna, G. Filippone, Interfacial crowding of nanoplatelets in Co-continuous polymer blends: assembly, elasticity and structure of the interfacial nanoparticle network, *Soft Matter* 13 (37) (2017) 6465–6473.
- [58] M. Mohammadi, C. Bruel, M.C. Heuzey, P.J. Carreau, CNC dispersion in PLA and PBAT using two solvents: morphological and rheological properties, *Cellulose* 27 (17) (2020) 9877–9892.
- [59] R. Al-Itry, *Blends Based on Poly(Lactic Acid) : Structure/Rheology/Processing Relationship*, 2012.
- [60] E. Vatanever, D. Arslan, D.S. Sarul, Y. Kahraman, G. Gunes, A. Durmus, M. Nofar, Development of CNC-reinforced PBAT nanocomposites with reduced percolation threshold: a comparative study on the preparation method, *J. Mater. Sci.* 55 (32) (2020) 15523–15537.
- [61] E. Vatanever, D. Arslan, D.S. Sarul, Y. Kahraman, M. Nofar, Effects of molecular weight and crystallizability of polylactide on the cellulose nanocrystal dispersion quality in their nanocomposites, *Int. J. Biol. Macromol.* 154 (2020) 276–290.
- [62] P. Pötschke, D.R. Paul, formation of Co-continuous structures in melt-mixed immiscible polymer blends, *J. Macromol. Sci. Polym. Rev.* 43 (1) (2003) 87–141.
- [63] **HSPiP FAQ | Hansen Solubility Parameters** <https://www.hansen-solubility.com/HSPiP/faq.php> (accessed Feb 23, 2021).